

Initiation of motility on a compliant substrate

Jocelyn Étienne^a, Pierre Recho^{a,*}

^a *Université Grenoble Alpes, CNRS, LIPHY, 38000 Grenoble, France*

Abstract

The conditions under which biological cells switch from a static to a motile state are fundamental to the understanding of many healthy and pathological processes. In this paper, we consider a cell constrained to move along a one-dimensional track. We show that even in the presence of a fully symmetric protrusive activity at the cell edges, such a spontaneous transition can result from a feedback of the deformation of an elastic substrate on the cell traction forces. The loss of symmetry of the traction forces leading to the cell propulsion is rooted in the fact that the surface loading follows the substrate deformation, leading the cell to surf its own wake. The bifurcation between the static and motile states is characterized analytically and, considering the measurements performed on two cell types, we show that such an instability can realistically occur on soft *in vivo* substrates.

1. Introduction

Most living cells have the ability to move to perform collective tasks necessary to vital biological functions such as wound healing or the immune response. To do so, they rely on their cytoskeleton, an active biopolymer meshwork that consumes chemical energy to locally contract and turnover [8]. Simple continuum models have been used to physically understand how either non-uniform contractility driven by molecular motors or material turnover due to the cytoskeleton polymerization and depolymerization can drive cell crawling by producing asymmetric traction forces on the cell substrate [31, 41, 11, 5, 55, 21, 12]. Moreover, starting from a static state, cells on stiff substrates can spontaneously initiate their motion by breaking the symmetry of their locomotion apparatus [64, 65, 3], following for instance a chemomechanical instability forming a pattern [46, 15, 38], dynamically modulating the adhesion [61] or the polymerization [56], or through a material instability whereby the active stress created by some molecular motors self-amplifies the cell cytoskeleton flow [53, 63, 10, 26]. It has also been shown that a cell formed of an isotropic gel, with constant surface polymerization and bulk depolymerization, can break its initially symmetric configuration through a morphological instability when the protrusive forces overcome the membrane resistance [7]. However, such an instability requires a two-dimensional shape and has no analogue for cells constrained to move along a narrow track, either at the surface of a substrate [44, 45] or inside a capillary [27] which is the framework considered in this paper. Interestingly, it has been argued that motility confined to such 1D structures may be closer to the physiological 3D motility in Extra-Cellular Matrices (ECM) than 2D motility on a flat substrate [20, 19].

In this paper, we show that substrate deformation can lead to symmetry breaking through a mechanical feedback that initiates the motion of a cell with symmetric boundary polymerization and bulk depolymerization. In many existing models of mechanotaxis, the observed influence of the substrate stiffness or deformation on cell motility [42, 22] is included through various mechanosensing pathways controlling the cell adhesion [39, 43, 24, 60, 13], the molecular motors' active stress [2, 62] or the cytoskeleton polymerization rate [66, 47]. In contrast, rather than mechanosensing, it is here the action and reaction at the cell-substrate interface which is at the origin of the spontaneous cell polarization. Indeed, the coupling of the internal cell dynamics and the substrate deformation is shown to result in a 'follower load' instability [6].

The paper is structured as follows. In Sec. 2, we introduce the mechanical model describing the flow of the cell cytoskeleton based on material turnover and its frictional interaction with the substrate. We then show in Sec. 3 that the treadmilling motion of the cytoskeleton makes it possible to transport the cell with an externally imposed substrate deformation. Considering in Sec. 4 a semi-infinite incompressible elastic

*Corresponding author

Email addresses: jocelyn.etienne@univ-grenoble-alpes.fr (Jocelyn Étienne), pierre.recho@univ-grenoble-alpes.fr (Pierre Recho)

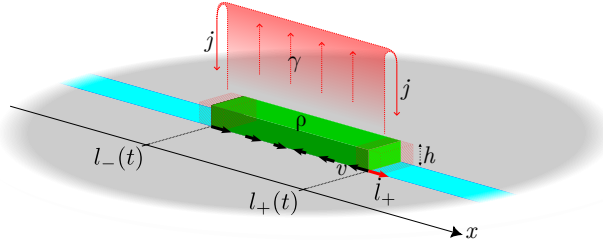


Figure 1: Schematic of the active gel segment on a track (light blue) subjected to a symmetric polymerization flux balanced by bulk depolymerization.

substrate under small deformations, which are now due to the traction forces of the cell itself, we show in Sec. 5 that when the cell-generated protrusive forces exceed a finite threshold, the static and symmetric state becomes unstable to the benefit of a polarized motile state. This instability occurs within the range of realistic material parameters values but features a substrate deformation field that is not admissible, as it implies matter self-penetration. It is then shown in Sec. 6 that this degenerate situation can be eliminated without compromising the instability when considering a biologically relevant non-linear friction case. Finally in Sec. 7, using a simpler Winkler-type model where the substrate consists of an elastic film anchored to a stiff foundation, we analyse the influence of large deformations which automatically prevent matter self-penetration. We show again that this does not qualitatively compromise the cell polarization instability described in Sec. 5. Interestingly, it is also shown that non-linear substrate deformations can lead to a reentrant behavior whereby the cell can spontaneously polarize and then depolarize as the symmetric protrusive forces increase.

2. Model of the cell skeleton: treadmilling-driven retrograde flow

We consider an active gel slab [34, 33] moving along a one-dimensional track, modeling the biopolymer meshwork of a cell crawling on a fibronectin-coated track. Neglecting inertial effects, the momentum balance in the gel reads

$$h\partial_x\sigma = f, \quad (1)$$

where h is the constant gel height, $\sigma(x, t)$ is the axial stress in the gel and $f(x, t)$ is the traction force applied by the cell on the substrate. The spatial coordinate of material points in the gel at time t is denoted $x \in [l_-(t), l_+(t)]$, where $l_-(t)$ and $l_+(t)$ are the moving fronts of the gel. We denote by $C(t) = (l_-(t) + l_+(t))/2$ the segment center and by $L(t) = l_+(t) - l_-(t)$ its length. In the absence of any external loading at the segment ends, the stress vanishes at the cell boundaries,

$$\sigma(l_{\pm}(t), t) = 0. \quad (2)$$

In order to clarify the physical ingredients at play in the instability that we shall present, we voluntarily neglect the active stress due to the presence of molecular motors and consider only the activity due to the meshwork polymerization at the boundaries and its depolymerization in the bulk. Mass balance within the gel reads [34]

$$\dot{\rho} + \rho\partial_x v = -\gamma\rho, \quad (3)$$

where $\rho(x, t)$ is the mass density of the gel and γ is a bulk depolymerization rate. The superimposed dot $\dot{\cdot} = \partial_t + v\partial_x$ denotes the total time derivative. This bulk mass conservation equation is associated with the boundary conditions:

$$\rho(l_{\pm}(t), t)(v(l_{\pm}(t), t) - \dot{l}_{\pm}) = \pm j, \quad (4)$$

where $j < 0$ is a fixed and *symmetric* polymerization flux at the two cell ends. See schematic in Fig. 1.

The constitutive behavior of the gel is modeled as an elastic solid at a short timescale. Hence, σ is a increasing function of the strain ρ_*/ρ that vanishes when $\rho = \rho_*$, the reference density of the biopolymer meshwork. See [52] for further discussion on the effective mechanical properties that arise in these conditions. As we explain below, due to our assumption that the relative density variations are small (see (6)), the specific dependence of the stress on the density of the gel is irrelevant in our analysis.

Combining the polymerization fluxes (4) with the absence of applied stress at the boundaries (2) which imposes $\rho = \rho_*$ there, we obtain the widely used kinematic conditions for the moving fronts [36, 33, 54, 7, 1]:

$$\dot{l}_{\pm} = \pm v_p + v(l_{\pm}(t), t), \quad (5)$$

where $v_p = -j/\rho_* > 0$ is a *symmetric* polymerization velocity at both ends [11, 55, 21].

Next, we assume that both the magnitude and rate of fluctuations of the gel density are small:

$$|\rho - \rho_*|/\rho_* \ll 1 \quad \text{and} \quad \dot{\rho}/\rho \ll \gamma \quad (6)$$

In this case, similarly to [7], (3) leads to $\partial_x v = -\gamma$. The cytoskeleton flow in the cell is then linear: $v(x, t) = -\gamma(x - l_-(t)) + \bar{v}(t)$, with $\bar{v}(t)$ a time-dependent function to be determined. This expression of velocity, combined with (5) leads to the following fronts dynamics: $\dot{L} = -\gamma L + 2v_p$ and $\dot{C} = \bar{v} - \gamma L/2$, showing that L converges to a steady state fixed value $L = L_{\text{eq}} = 2v_p/\gamma$ and that \bar{v} can be expressed as a function of \dot{C} :

$$v(x, t) = -\gamma(x - C(t)) + \dot{C}(t).$$

Such a symmetrically treadmilling system can be put into motion by a spatial asymmetry in its frictional interaction with the substrate [61, 56, 59] since the traction forces are then biased in one direction. We consider here a different situation where the friction coefficient ξ with the substrate is a constant but the traction forces depend on the relative velocity of the gel with respect to the substrate:

$$f = \xi \Psi_*(v - v_s). \quad (7)$$

In (7), v_s is the tangential velocity of the substrate surface along the track and Ψ_* is an odd function, which characterizes the non-linear behavior of the sliding friction between the gel and the substrate. This is relevant to cell migration, since the effective friction law is known to be biphasic [25] due to the stochastic collective dynamics of force-sensitive adhesive bonds [58, 60]. In what follows, we take the simple approximation

$$\Psi_*(v) = \frac{v}{1 + (v/v_*)^2},$$

which leads to a switch of behavior when the relative velocity reaches the threshold velocity v_* .

We aim at showing that the non-local feedback of the friction forces through the velocity v_s of a compliant substrate can lead to a symmetry breaking and spontaneous motility.

3. Externally actuated substrate

To first explain the physics of this motion, we start by considering the situation of a deformation imposed externally to a linear elastic incompressible substrate, which occupies the half space $z < 0$ below the cell. We assume that the deformation is created by the presence of magnetic beads at the substrate surface, along the track. The beads are actuated by an electromagnet of exactly the cell size L that is quasistatically moved along the track at a velocity V_e . As they are polarized in the z direction, the torque acting on the beads vanishes while they experience a traction force oriented only in the x -direction that takes the form $f_m = f_m^0 F(y(x, t))$, where the characteristic force f_m^0 scales with the current in the electromagnet and the beads magnetization and $y(x, t) = 2(x - V_e t)/L$ is the traveling wave coordinate. By asymptotic matching of the magnetic field (see [35], chap IV, paragraph 30) close and far from the magnet, we can approximate $F(y) = -y$ if $|y| < 1$ and $-y/|y|^5$ if $|y| > 1$. Next, restricting our analysis to small deformations, the substrate displacement at the surface $z = 0$ is purely tangential and takes the form of the traveling wave $u(x, t) = u^0 U(y(x, t))$ where, in plane strain, U reads (see [30] paragraph 2.4 for the derivation of this logarithmic plane strain kernel):

$$U(y) = - \int_{-\infty}^{\infty} \log |y - y'| F(y') dy', \quad (8)$$

and $u^0 = 3f_m^0 L / (2\pi E_s)$. The Young modulus of the substrate is denoted E_s .

In (8), we have neglected the contribution of the cell to the traction force acting on the substrate, assuming that $|f_m^0| \gg \xi v_p$. Using again the small deformation assumption, the substrate velocity is also a traveling wave given by $v_s = \partial_t u = -V_e \epsilon$ where the strain of the substrate surface is $\epsilon = \epsilon^0 E(y(x, t))$ with $E(y) = \partial_y U$

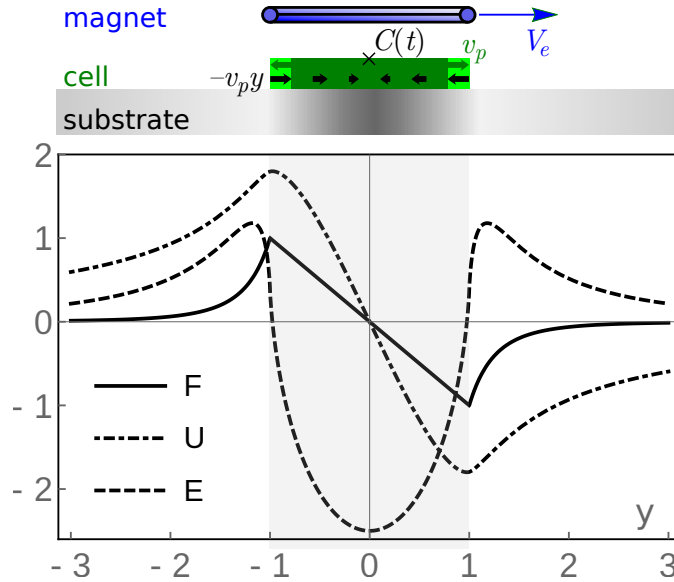


Figure 2: Top, an electromagnet moved at velocity V_e induces a mechanical strain (gray-coded) in a substrate. A cell is in frictional interaction with the substrate, it is assumed to treadmill with velocity $-v_p y$ and polymerize at its edges with speed v_p . Bottom, shape of the force applied by the magnet, displacement and strain of the elastic substrate surface.

and $\epsilon^0 = 3f_m^0/(\pi E_s)$. The functions F , U and E representing the spatial variations of the applied force, substrate displacement and strain along the track are shown in Fig. 2.

Finally, as the total force that is exerted on the treadmilling segment has to vanish, we obtain from (7) that

$$0 = - \int_{C(t)-L/2}^{C(t)+L/2} f(x)dx, \text{ which implies that, } 0 = \int_{-1}^1 \Psi_* \left(\dot{C}(t) - v_p y + V_e \epsilon^0 E(y + \delta(t)) \right) dy, \quad (9)$$

where $\delta(t) = y(C(t), t)$. Equation (9) is a differential equation that sets the $C(t)$ dynamics. Taking $C(0) = 0$ (the driving electromagnet is centered with the cell from the start) and since E decays to zero at infinity, the only permanent regime of motion is for $\delta(t) = 0$, i.e. a segment velocity equal to the actuation velocity $\dot{C} = V_e$: we call this mode of motion at the speed of the elastic wave ‘surfing’. Thus, (9) becomes the algebraic equation

$$0 = \int_{-1}^1 \Psi_* (-v_p y + V_e (1 + \epsilon^0 E(y))) dy, \quad (10)$$

that sets the strain magnitude ϵ^0 of the traveling wave such that it can be surfed by the treadmilling gel.

If Ψ_* is a linear function, this surfing condition becomes independent of V_e and v_p and simply reads $\bar{\epsilon} = \frac{1}{2} \int_{-1}^1 \epsilon(y) dy = -1$. Such an average elastic strain of the substrate is not admissible since it implies self-interpenetration of matter. Likewise, for non-linear Ψ_* , no solution exists if the treadmilling is slow, $v_p \ll V_e(1 - \epsilon^0)$. We thus focus on the case $v_p \gg V_e$. Since $\int_{-1}^1 \Psi_*(-v_p y) dy = 0$, a first order expansion leads to the surfing condition

$$0 = \int_{-1}^1 \Psi'_* (-v_p y) (1 + \epsilon(y)) dy. \quad (11)$$

The above condition, where $'$ denotes the derivative, shows the importance of the treadmilling dynamics and the non-linear friction for the surfing to be physically feasible. Indeed, the prefactor $\Psi'_*(-v_p y)$ has to change sign in order to make the cancellation of the integral possible for admissible $\bar{\epsilon} > -1$. The necessary and sufficient conditions for surfing motion are thus the presence of treadmilling and a biphasic friction Ψ_* . These conditions are in fact necessary whatever the origin of the substrate deformation.

4. The coupled problem

We now turn to the coupled problem asking whether the cell can surf on an elastic wave that it itself creates instead of relying on an external traveling wave driven by a moving magnetic field. We therefore express the

name	symbol	typical value
actin depolymerization rate	γ	0.03 s^{-1} [37, 57]
actin polymerization velocity	v_p	$0.25 \text{ } \mu\text{m s}^{-1}$ [57]
friction coefficient	ξ	$1 \text{ kPa s } \mu\text{m}^{-1}$ [57, 4]
saturation velocity	v_*	$0.125 \text{ } \mu\text{m s}^{-1}$ [3]
ECM Young modulus	E_s	100 Pa [40, 18]
characteristic length	$L = 2v_p/\gamma$	$17 \text{ } \mu\text{m}$
characteristic time	$1/\gamma$	33 s
characteristic velocity	$L\gamma$	$0.5 \text{ } \mu\text{m s}^{-1}$
characteristic stress	$2\xi v_p$	0.5 kPa
protrusive stress/substrate stiffness	$\theta = 3\xi v_p/(\pi E_s)$	2.5
traction forces saturation	$\beta = v_p/v_*$	2

Table 1: Rough estimates of the model parameters, characteristic scales and dimensionless parameters for fish keratocytes.

surface displacement in response to the cell traction forces themselves [30], which we had previously neglected compared to the action of the magnetic field:

$$u(x, t) = \frac{-3}{2\pi E_s} \int_{C(t)-L/2}^{C(t)+L/2} \log \left| \frac{x-x'}{L} \right| f(x', t) dx'. \quad (12)$$

Changing the time and space variables to follow the cell motion, $s = t$ and $y = 2(x - C(t))/L$, we have $\partial_t = \partial_s - (2\dot{C}/L)\partial_y$. Then, the velocity of the substrate for small deformations $v_s = \partial_t u$ can be expressed as a functional of the traction force distribution from (12):

$$v_s(y, s) = -\frac{3L}{4\pi E_s} \int_{-1}^1 \log |y - y'| \partial_s f(y', s) dy' + \frac{3\dot{C}(s)}{2\pi E_s} \int_{-1}^1 \frac{f(y', s)}{y - y'} dy'. \quad (13)$$

In these coordinates, the cell cytoskeleton's velocity is

$$v(y, s) = -v_p y + \dot{C}(s). \quad (14)$$

Non-dimensionalizing the distance by L , the time by $1/\gamma$ and the stress by $2\xi v_p$, and defining the non-dimensional substrate displacement and strain ($\epsilon = \partial_x u$):

$$u[f](y, s) = -\frac{\theta}{2} \int_{-1}^1 \log |y - y'| f(y', s) dy' \quad \text{and} \quad \epsilon[f](y, s) = -\theta \int_{-1}^1 \frac{f(y', s)}{y - y'} dy', \quad (15)$$

the three relations (7), (13) and (14) are combined in a single non-linear integral equation that determines the distribution of the cell traction forces,

$$2\beta f = \Psi \left(2\beta(\dot{C} - y/2 - u[\partial_s f] + \dot{C}\epsilon[f]) \right), \quad (16)$$

with $\Psi(v) = v/(1 + v^2)$. The non-dimensional parameters of the model, respectively

$$\beta = \frac{v_p}{v_*} \quad \text{and} \quad \theta = \frac{3\xi v_p}{\pi E_s},$$

represent the level of importance of the non-linearity of the sliding friction law ($\beta \ll 1$ being the linear viscous friction limit, either because v_* is large or because v_p is small) and the stress imposed by the protrusion compared to the elastic modulus of the substrate. Rough estimates of these model parameters, characteristic scales and non-dimensional parameters in the well studied case of fish keratocytes are compiled in Table 1. Equation (16) also depends on the unknown crawling velocity \dot{C} , which is set by the global force balance condition

$$\int_{-1}^1 f(y, s) dy = 0. \quad (17)$$

When the substrate is infinitely rigid ($\theta = 0$), our model (16) directly provides the expression of the traction forces $f = \Psi(2\beta(\dot{C} - y/2))/(2\beta)$ and (17) necessarily implies that $\dot{C} = 0$. Therefore, as can be expected for a system with symmetric polymerization at both ends, in the absence of intra-cellular feedbacks of the type considered in [56, 61] (a polarization of the adhesion molecules concentration in [61] and an inhibitor of polymerization in [56]), the steady state traction force profile $f_0(y) = \Psi(-\beta y)/(2\beta)$ is always symmetric with respect to the cell center and the cell always remains static. While such a distribution remains a solution of the integral problem (16)-(17), one can note the presence of the nonlinear term $\dot{C}\epsilon[f]$ in (16). This term finds its origin in the time evolution of the substrate deformation due to the dynamics \dot{C} of the interval over which the load f is applied on the substrate, and thus of the motion of the cell itself. We now proceed to examine the stability of this system.

5. Linear friction

To do so, we begin by investigating the situation when $\beta \ll 1$ (the sliding friction law is linear) and (16) reduces to the linear integral equation on the distribution f :

$$f = \dot{C} - y/2 - u[\partial_s f] + \dot{C}\epsilon[f]. \quad (18)$$

Notice however that (18) still contains an implicit non-linearity in its last term as \dot{C} is a functional of f fixed by (17). We show below that the presence of this crucial term, which advects the substrate deformation with the cell motion, is the root of spontaneous motility in this system.

Inserting in (18) the perturbation of the static solution with a growth rate λ ,

$$f(y, s) = f_0(y) + \eta e^{\lambda s} \delta f(y) \quad \text{and} \quad \dot{C} = \eta e^{\lambda s} \delta \dot{C},$$

we find, at first order in the small parameter η , that $\delta f(y) = \delta \dot{C}(1 + \epsilon[f_0(y)]) - \lambda u[\delta f(y)]$. Imposing the global force balance condition (17), $\delta \dot{C}$ is expressed as a functional of δf to obtain,

$$\left(2 + \int_{-1}^1 \epsilon[f_0] dy\right) \frac{\delta f}{\lambda} = (1 + \epsilon[f_0]) \int_{-1}^1 u[\delta f] dy - \left(2 + \int_{-1}^1 \epsilon[f_0] dy\right) u[\delta f]. \quad (19)$$

When θ is small, multiplying (19) by δf and integrating, leads to

$$\int_{-1}^1 (\delta f(y))^2 dy = \frac{\lambda \theta}{2} \int_{-1}^1 \int_{-1}^1 \log |y - y'| \delta f(y) \delta f(y') dy dy'.$$

As the linear operator $u[f]$ is symmetric positive definite [23], we conclude from the above equation that λ is negative and the static steady state is stable to small perturbations for $\theta \ll 1$. This limiting behavior also shows that, in general, the u term in (18) describing the elastic feedback of the substrate when the loading domain is fixed does not destabilize the central symmetry of the traction forces in the static configuration and thus does not contribute to making the system motile. However, the growth rate of the instability can vanish ($\lambda = 0$) when θ reaches a critical threshold θ_c in (19) that satisfies the condition $2 + \int_{-1}^1 \epsilon[f_0] dy = 0$, leading to $\theta_c = 2$. Close to this threshold, the behavior of $\lambda(\theta)$ can be expanded in power series and we find at first order that $\lambda \sim 9(\theta - \theta_c)/(2(\pi^2 - 6))$, showing that the growth rate of a perturbation of the static solution becomes positive beyond $\theta = \theta_c$. Thus, the contribution of the substrate deformation due to the fact that the loading domain moves if the cell moves (so-called ‘follower load’ effect [6]) makes the static state unstable when the traction forces compared to the substrate elasticity increase beyond the critical threshold θ_c .

The post-bifurcation regime can be characterized analytically by searching traveling wave solutions of (18) for which $\partial_s f = 0$ and $V = \dot{C}$ is a constant. Indeed, the Cauchy integral equation:

$$\theta V \int_{-1}^1 \frac{f(y')}{y - y'} dy' + f(y) = -\frac{y}{2} + V, \quad (20)$$

has an integrable solution which reads [32]:

$$f_{\text{eq}}(y) = -\frac{(y/2 + V)w_a(y)}{\sqrt{1 + (\theta\pi V)^2}}, \quad (21)$$

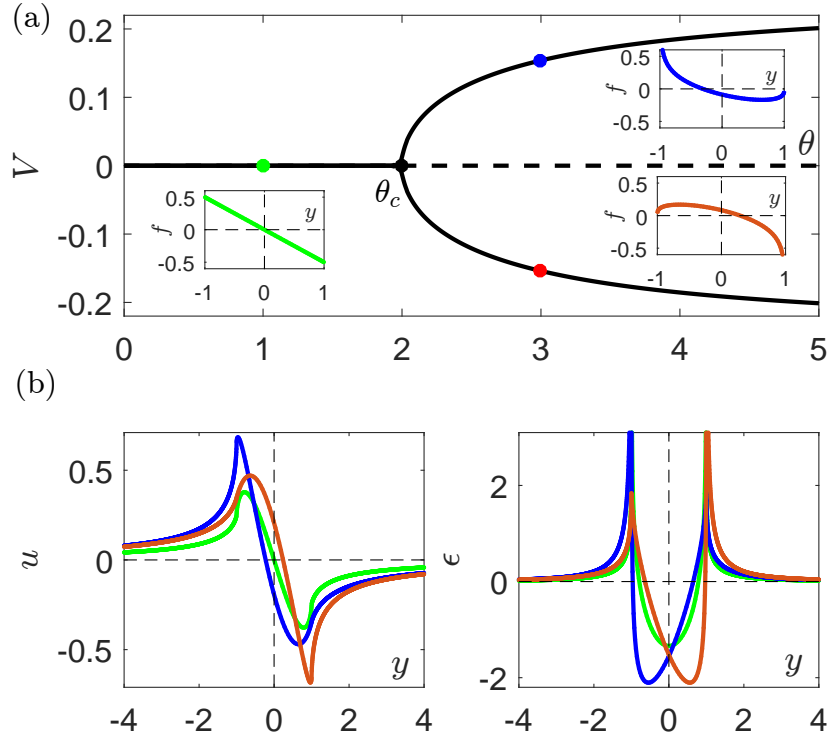


Figure 3: (a) Static to motile transition for a linear sliding friction law (Eq. (20)). Characteristic traction forces profiles (21) are shown in inserts. The static branch is dashed passed the critical point $\theta = \theta_c$ since it becomes unstable. (b) Profiles of the substrate displacement and strain corresponding to the traction forces shown in (a)

where $w_a(y) = ((1-y)/(1+y))^a$ and $a = \arctan(\theta\pi V)/\pi$. Thus, imposing the global force balance condition (17), we find that the cell velocity satisfies the implicit relation:

$$V = a/2 = \arctan(\theta\pi V)/(2\pi). \quad (22)$$

If $\theta \leq \theta_c = 2$, equation (22) has the single root $V = 0$ (stable static solution) while if $\theta > \theta_c$, it has three roots: $V = 0$ corresponding to the now unstable static configuration and the two others corresponding to two symmetric motile configurations, see Fig. 3(a).

Using the model parameters estimates for fish keratocytes collected in Table 1, we find a value of $\theta \simeq 2.5$, close to θ_c , for a substrate with a Young modulus of $E_s \simeq 100$ Pa, which is within the range of stiffnesses of ECM measured *ex-vivo* [40] and *in vitro* [18]. This suggests that the present motility initiation instability could realistically be at play following a uniform actin polymerization activation at the membrane for *in vivo* soft substrates. Upon the bifurcation, the symmetry of the traction forces is lost (insets of Fig. 3(a)) with a maximum at the trailing edge and a negative part at the leading edge in qualitative agreement with experiments [28]. This in turn leads to an asymmetric substrate displacement and strain (see Fig. 3(b)) that promotes the cell motion, which ‘surfs’ on the deformation it creates. Conceptually, this can be likened to the “walker droplets” that are made to bounce on a liquid bath [51] with an external actuation. Such bouncing generates a surface wave and, beyond a threshold of forcing, the droplet starts to propagate at a constant velocity due to its interaction with the wave it produces. Yet another example of spontaneous polarization where, contrary to our framework, inertial forces play an important role is that of a bristle-bot robot driven by an oscillating force [16, 14]. In this case, it is the dynamical dependence of the friction coefficient itself on the normal component of the traction force that leads to directional motility through a stick-slip instability. By simulating numerically (18), we show in Fig. 4 the robust convergence of the cell to the aforementioned steady state configurations regardless of initial conditions, in line with the small perturbation stability results.

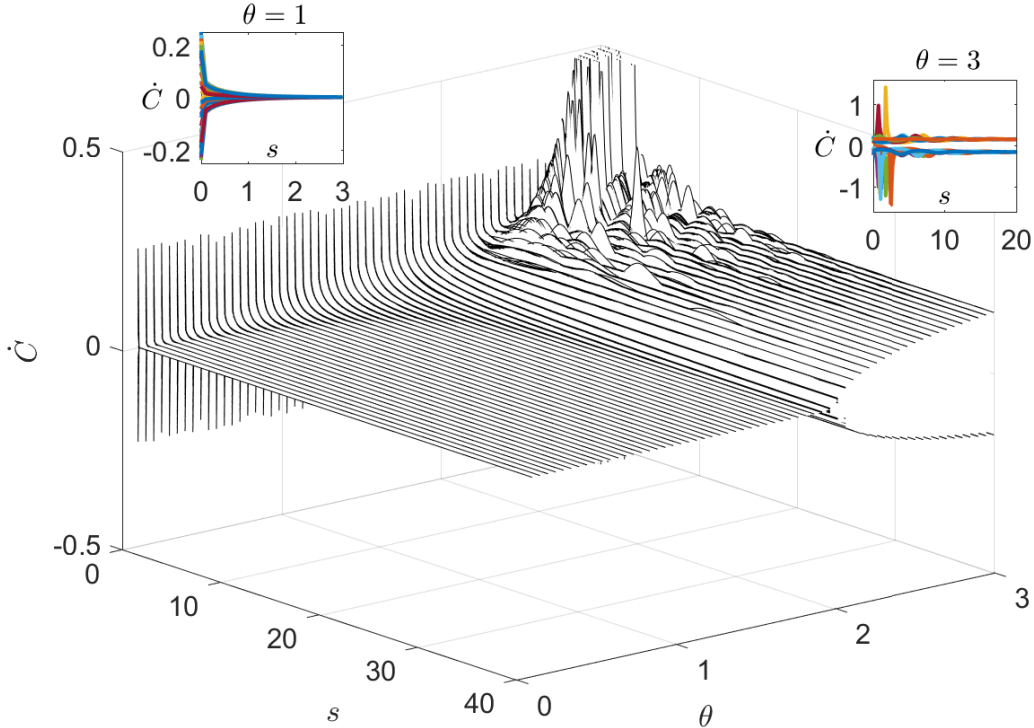


Figure 4: Convergence of the instantaneous cell velocity found from (18) to its steady state value predicted by (22) for an initial traction force profile of the form of (21) but with an initial velocity randomly chosen in the interval $[-0.25, 0.25]$ (corresponding to the maximal velocity in (22)). Large transient oscillations can arise before reaching the steady state velocity.

6. Non-linear friction

Although the above results with a linear friction law limit ($\beta \ll 1$) allow to characterize the physics of substrate deformation-induced motility initiation, the instability arises in a parameter range for which the deformation is not physically admissible. Indeed, as in the case of externally imposed deformations that has been presented in Sec. 3, the surface strain at the bifurcation threshold $\epsilon_c(y) = 2(y \log(\sqrt{|(1+y)/(1-y)|}) - 1)$ has values below -1 over a finite interval. We now show that here too, a biphasic sliding friction (finite β) restores the possibility of an admissible substrate deformation. In this case, the perturbation of the static state leads to

$$\delta f(y) = \Psi'(-\beta y)(\delta \dot{C}(1 + \epsilon[f_0(y)]) - \lambda u[\delta f(y)]) \quad (23)$$

and the growth rate of the perturbation switches from a negative to a positive value at the critical value:

$$\theta_c(\beta) = \frac{4(\beta^2 + 1)}{(\beta^{-2} + 1) \arctan(\beta) ((\beta^2 + 1) \arctan(\beta) + 2\beta) - 1}. \quad (24)$$

The strain at the bifurcation threshold reads

$$\epsilon_c = -\theta_c(\beta) \frac{\beta y \log \left| \frac{1-y}{1+y} \right| + 2 \arctan(\beta)}{2(\beta + \beta^3 y^2)},$$

which approaches zero when β increases except in narrow boundary layers at $y = \pm 1$ close to the cell fronts. This leads to an average strain under the gel $\bar{\epsilon}_c = \frac{1}{2} \int_{-1}^1 \epsilon_c(y) dy = -\theta_c(\beta) \arctan^2(\beta) / (2\beta^2)$, that tends to zero as $\beta \rightarrow \infty$. Thus for a large enough β , the critical value of θ at which the bifurcation happens predicted by (24) becomes small and the small deformations assumption is also verified. For fish keratocytes, the value of $v_* \simeq 0.125 \mu\text{m s}^{-1}$ in the biphasic relation was estimated in [3] based on experiments on stiff substrates, leading to $\beta \simeq 2$ and $\bar{\epsilon}_c \simeq -0.25$. The biphasic relation was also initially characterized for another cell type (PtK1). In this case, the polymerization velocity can be estimated from [50] to be $v_p \simeq 0.03 \mu\text{m.s}^{-1}$

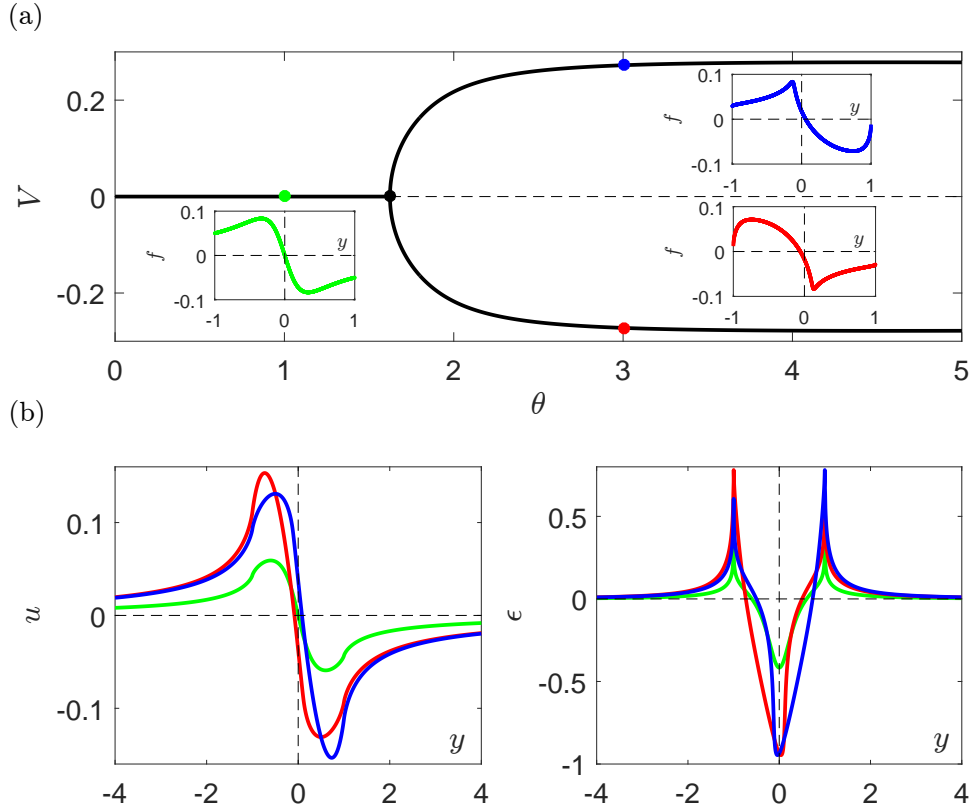


Figure 5: (a) Pitchfork bifurcation of the segment steady state velocity from a static to a motile state for the non-linear system (16)-(17). Typical traction forces distributions for special choices of θ (same as for Fig. 3) are shown in inset. (b) Substrate displacement and strain associated to the traction forces profiles shown in (a). Parameter $\beta = 3$.

and the data of [25] indicates an effective friction coefficient of $\xi \simeq 10 \text{ kPa}\cdot\text{s}\cdot\mu\text{m}^{-1}$ and a threshold velocity $v_* \simeq 0.01 \mu\text{m}\cdot\text{s}^{-1}$. This leads to non-dimensional parameters $\theta \simeq 3$ and $\beta \simeq 3$ and to $\bar{\epsilon}_c \simeq -0.15$.

We compute by numerical continuation the traction force profile and the cell velocity beyond the bifurcation threshold for this more realistic sliding friction law, see Fig. 5. The traction force profiles are similar to the ones of the linear case except that their divergence at the trailing edge is eliminated because of the thresholding effect of Ψ . The cell-generated substrate displacement is also similar to the linear case, albeit smaller, leading to admissible strain profiles that satisfy $\epsilon > -1$. Using the model parameters estimated in Table 1, we find at $\theta = 2.5$ and $\beta = 2$, a crawling velocity of the order of $\sim 0.1 \mu\text{m s}^{-1}$ similar to the one experimentally observed on stiff unconfined substrates ($\sim 0.2 \mu\text{m s}^{-1}$ [57]). The typical order of magnitude of the traction forces that reach $\sim 50 \text{ Pa}$ is also comparable to the measurements performed in the aforementioned conditions which give 100 Pa [57]. While our model is not meant to reproduce quantitatively a specific experiment but rather to capture the physical ingredients necessary to observe an instability, matching the correct order of magnitude for these quantities suggests that the described spontaneous polarization mechanism is indeed applicable to cell motility.

7. Influence of large substrate deformations

Equation (12) and the relation $v_s = \partial_t u$ rely on the assumption that the substrate deformation remains small. Even in the presence of a realistic non-linear friction law (finite β), the substrate strain can locally reach values where this simplifying assumption becomes questionable. See Fig. 5 (b). In this section, considering a different model for the elastic substrate amenable to a semi-analytic analysis, we show that the protrusion-driven spontaneous motility initiation that we have evidenced in the previous sections occurs following an instability that is qualitatively unchanged when allowing large substrate deformations.

To do so, instead of relating the substrate displacement to the applied traction forces using formula (12), we consider a Winkler–Pasternak type foundation model [48] where the ECM substrate is an elastic film

subjected to tangential loading and elastically adhering to a stiff foundation, leading to

$$-E_s \Phi'(1 + \partial_X u) \partial_{XX} u + \frac{G}{l^2} u = f,$$

where E_s is the modulus of the film modeling the ECM, Φ is the non-linear stress-strain dependence ($'$ denotes its derivative), l the film thickness and G is the shear modulus of the connection to the foundation. Importantly, X is the Lagrangian spatial coordinate along the track in the reference (stress-free) configuration of the substrate. As a consequence, in Eulerian variables (current configuration) we have, $\partial_X u = (1 + \partial_x u) \partial_x u$ and $v_s = \partial_t u + v_s \partial_x u$. Thus, the strain being $\epsilon = \partial_X u$ we have,

$$\epsilon = \frac{\partial_x u}{1 - \partial_x u} \quad \text{and} \quad v_s = \frac{\partial_t u}{1 - \partial_x u}.$$

In order to allow large deformations, we use the true strain $\Phi(1 + \epsilon) = \log(1 + \epsilon)$ as this choice naturally restricts deformations to the admissible domain, $\epsilon > -1$. We obtain,

$$\begin{cases} -E_s \partial_x \epsilon + \frac{G}{l^2} u = f \\ (1 + \epsilon) \partial_x u = \epsilon. \end{cases} \quad (25)$$

The above non-linear relation between f and u replaces (12). As a result, in non-dimensional form and with the change of variable from (x, t) to (y, s) , the analogue of the model of small deformation of a semi-infinite substrate (16) is:

$$\begin{cases} -2\partial_y \epsilon + r\alpha^2 u = \frac{\pi\alpha\theta}{6\beta} \Psi \left(2\beta(\dot{C} - y/2 - (1 + \epsilon)(\partial_s u - 2\dot{C}\partial_y u)) \right) \mathbf{1}_{[-1,1]}(y) \\ 2(1 + \epsilon)\partial_y u = \epsilon, \end{cases} \quad (26)$$

where the additional non-dimensional parameters

$$r = \frac{G}{E_s} \quad \text{and} \quad \alpha = \frac{L}{l}$$

represent the shear adhesion strength of the substrate to the foundation compared to the film elasticity and the cell length compared to the film thickness. The notation $\mathbf{1}_{[-1,1]}$ denotes the indicator function of the segment $[-1, 1]$ where the traction forces are non vanishing. The substrate displacement u is continuous across these points as well as the strain ϵ (due to stress continuity in the substrate). At $y = \pm\infty$, we impose the static conditions $u = 0$ and $\epsilon = 0$. Solving (26) in quadrature in the two side domains where the traction forces vanish and using the continuity conditions, we reduce (26) to the interval $[-1, 1]$ with the appropriate boundary conditions and seek for traveling wave solutions for which $\dot{C} = V$ is a constant and $\partial_s u \equiv 0$:

$$\begin{cases} -2\partial_y \epsilon + r\alpha^2 u = \frac{\pi\alpha\theta}{6\beta} \Psi(2\beta((1 + \epsilon)V - y/2)) \\ 2(1 + \epsilon)\partial_y u = \epsilon \\ r\alpha^2 u(\pm 1)^2/2 = \epsilon(\pm 1) - \log(1 + \epsilon(\pm 1)). \end{cases} \quad (27)$$

We solve (27)-(17) for (V, u, ϵ) by numerical continuation [17] starting from the trivial solution $V = 0$, $u \equiv 0$ and $\epsilon \equiv 0$ when $\theta = 0$.

The situation is qualitatively similar to the one shown in Fig. 5 when the substrate is modeled as an elastic incompressible semi-infinite material under small deformations: there exists a critical value of θ at which the symmetric and static state loses its stability to initiate an asymmetric traveling solution corresponding to a motile state. The obtained traction forces and substrate displacement profiles are also comparable, showing that the cell polarization instability that we describe in this paper is consistently due to mechanisms independent of the small deformation assumption. Interestingly, in the post-bifurcated regime, the velocity dependence as a function of the substrate stiffness is not monotonic and displays a maximum for a particular substrate stiffness as observed in some experiments [49]. Together with [12], these results indicate that this experimental observation may be explained by the emergent effect of non-local coupling of traction forces via the compliant substrate.

Furthermore, we show in Fig. 7 (a) the dependence of the critical value θ_c at the bifurcation threshold for fixed parameters α and r . As expected, when β becomes sufficiently small, corresponding to a linear friction regime, we do not find any critical θ_c corresponding to the motility initiation instability, contrarily to what

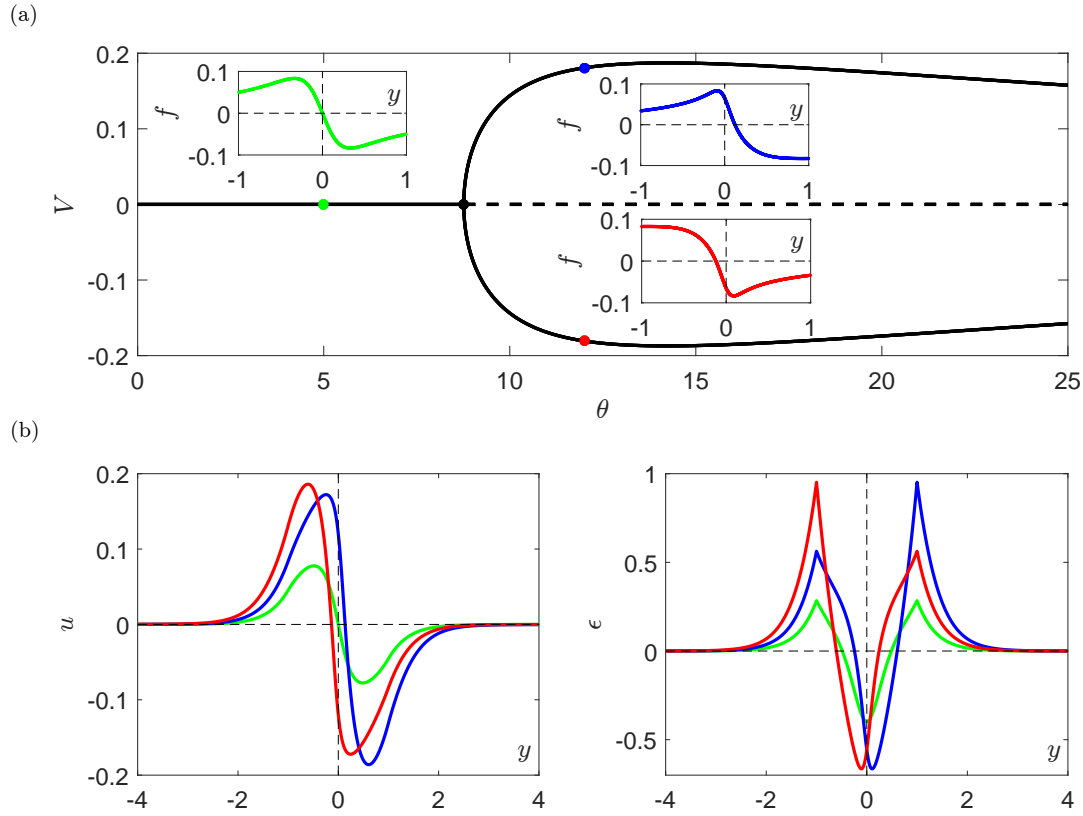


Figure 6: (a) Bifurcation from a static to a motile state at a critical value of θ with the simplified model of the elastic foundation (27). We show in insets the traction forces profiles along the three branches at the points labeled with the related colored dots. (b) Substrate displacement and deformation along the three branches (color corresponds to the dots in (a)). Parameters $\beta = 3$, $r = 0.3$ and $\alpha = 10$.

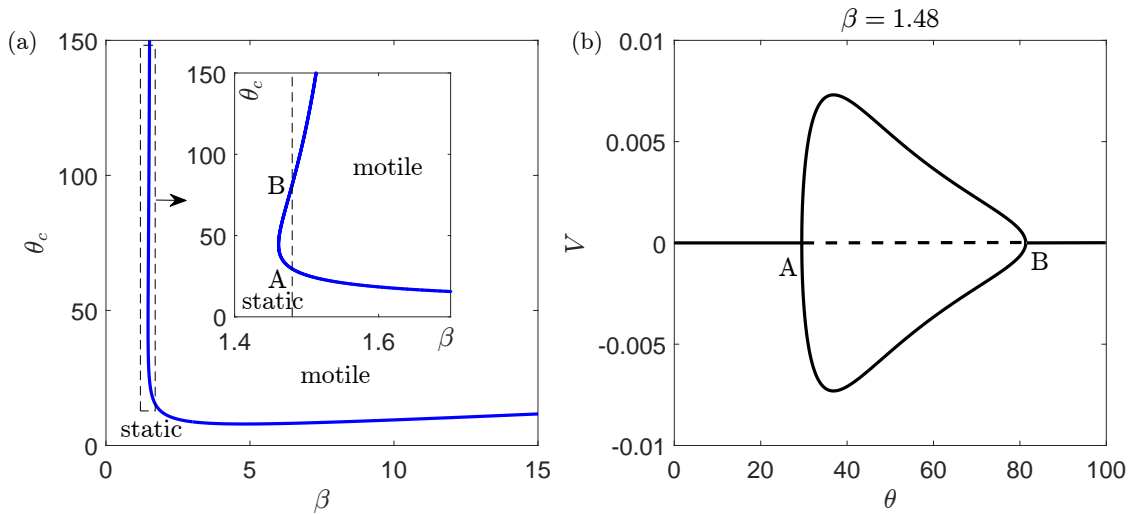


Figure 7: (a) Locus of the bifurcation point between the static and motile solutions in the parameter space (β, θ) . Inset shows the turning point. Points A and B are related to the bifurcation diagram shown on the right panel. (b) Bifurcation diagram showing an isola center type bifurcation at $\beta = 1.48$ where the segment first polarizes at point A and then depolarizes at point B while the control parameter θ keeps increasing. Parameters $\alpha = 10$ and $r = 0.3$.

is observed in Sec. 5. This is because in the model (27) rules out matter self-penetration, which according to condition (11) is necessary to obtain surfing with a linear friction. Instead, we observe a turning point in the dependence of θ_c on β (Fig. 7 (a) inset) and the spontaneous motility instability is restricted to finite values of β . Due to the existence of this turning point, for a range of β , the bifurcation can be of isola center type with a depolarization and reconnection to the static branch following the motility initiation. See Fig. 7 (b). The motility regime is therefore restricted to a finite range of substrate stiffness with neither too stiff nor too soft substrates enabling motility initiation in this case. This qualitative result further underlines the potential role that non-linear elasticity of the substrate may play in the interpretation of experimental results showing a biphasic dependence of the cell velocity as a function of the substrate stiffness [49].

8. Conclusions

We have shown that symmetric protrusions driving the cell cytoskeleton flow can initiate spontaneous cell motility on a soft substrate. This instability requires two well-established non-linearities that we have deliberately selected among others to obtain our minimal model. First, a geometric non-linearity that finds its origin in the advection of the substrate strain with the cell motion. Thereby, the cell surfs on the substrate deformation it creates. The feedback between the substrate and the cell mechanics is fully mediated by the frictional traction forces and requires no specific mechanosensing, which suggests that this phenomenon could be universal across cell types. However, the physical admissibility of the motile configuration requires a second non-linearity of material type in the effective sliding friction interaction between the cell and the substrate. This experimentally established biphasic behavior [25] eliminates the spurious matter self-penetration beyond the instability threshold, although this ingredient is not needed to understand the instability in itself. Considering large deformations in the substrate confirms the robustness of the mechanism of the cell polarization transition and unravels a more complex bifurcation diagram than in the small deformation case, with the possibility of a biphasic dependence of the cell velocity as a function of the substrate stiffness.

Even though experimentally challenging, future work could aim at deciding whether the substrate compliance increases significantly the frequency of motility initiation as it was done in [3] to investigate the role of various drugs on motility initiation. Indeed, on glass, constraining keratocytes to move along narrow adhesive $5\mu\text{m}$ tracks led to circa 98% of immobile cells in [45]. Combining soft substrates and narrow tracks could thus allow to test our model. Qualitatively, the bifurcation threshold (24) indeed states that when the magnitude of the traction forces due to protrusive stress becomes of the same order as the substrate stiffness, there is a transition from a static to a motile state. As Traction Force Microscopy allows to quantify these stresses [45] and microfabrication makes it possible to produce substrates with a corresponding elastic modulus [12], this suggests a path to experimentally find a critical substrate softness beyond which a given cell type starts to move along a track.

To be more quantitative and comprehensive, this model could be enriched with other mechanisms of self-polarization on one dimensional tracks, such as contraction-driven motility [53] that can also operate for infinitely stiff substrates. It could also be coupled to internal cell signaling, controlling the local protrusion rates at the cell boundary as a function of Rho GTPases concentration that undergo reaction-drift-diffusion dynamics in the cytoplasm [46], further enhancing the cell polarity when the symmetry of the internal flow is broken [1, 56].

Another interesting generalization to reach a more quantitative model of a specific experiment would be to represent the substrate rheology and the track geometry in a refined way [12]. Finally, the coupling between fluctuations of the internal cytoskeleton dynamics and the confining geometry [9] and stiffness [29] of the cell environment is also known to play an important role in cell motility.

Acknowledgments

The authors thank L. Truskinovsky for his stimulating comments, as well as Alexander Erlich for his critical and helpful reading of the manuscript.

References

- [1] Ambrosi, D., Zanzottera, A., 2016. Mechanics and polarity in cell motility. *Physica D* , 58–66doi:10.1016/j.physd.2016.05.003.

- [2] Banerjee, S., Marchetti, M.C., 2011. Substrate rigidity deforms and polarizes active gels. *EPL (Europhysics Letters)* 96, 28003.
- [3] Barnhart, E., Lee, K.C., Allen, G.M., Theriot, J.A., Mogilner, A., 2015. Balance between cell-substrate adhesion and myosin contraction determines the frequency of motility initiation in fish keratocytes. *Proceedings of the National Academy of Sciences* 112, 5045–5050.
- [4] Barnhart, E.L., Lee, K.C., Keren, K., Mogilner, A., Theriot, J.A., 2011. An adhesion-dependent switch between mechanisms that determine motile cell shape. *PLoS biology* 9, e1001059.
- [5] Bergert, M., Erzberger, A., Desai, R.A., Aspalter, I.M., Oates, A.C., Charras, G., Salbreux, G., Paluch, E.K., 2015. Force transmission during adhesion-independent migration. *Nature cell biology* 17, 524–529.
- [6] Bigoni, D., Noselli, G., 2011. Experimental evidence of flutter and divergence instabilities induced by dry friction. *Journal of the Mechanics and Physics of Solids* 59, 2208–2226.
- [7] Blanch-Mercader, C., Casademunt, J., 2013. Spontaneous motility of actin lamellar fragments. *Physical review letters* 110, 078102.
- [8] Boal, D., 2012. *Mechanics of the Cell*. 2 ed., Cambridge University Press. doi:10.1017/CB09781139022217.
- [9] Buskermolen, A.B., Suresh, H., Shishvan, S.S., Vigliotti, A., DeSimone, A., Kurniawan, N.A., Bouten, C.V., Deshpande, V.S., 2019. Entropic forces drive cellular contact guidance. *Biophysical journal* 116, 1994–2008.
- [10] Callan-Jones, A., Voituriez, R., 2013. Active gel model of amoeboid cell motility. *New Journal of Physics* 15, 025022.
- [11] Carlsson, A., 2011. Mechanisms of cell propulsion by active stresses. *New journal of physics* 13, 073009.
- [12] Chelly, H., Jahangiri, A., Mireux, M., Étienne, J., Dysthe, D., Verdier, C., Recho, P., 2022. Cell crawling on a compliant substrate: a biphasic relation with linear friction. *International Journal of Non-Linear Mechanics* 139, 103897.
- [13] Chen, P.C., Feng, X.Q., Li, B., 2022. Unified multiscale theory of cellular mechanical adaptations to substrate stiffness. *Biophysical Journal* 121, 3474–3485.
- [14] Cicconofri, G., DeSimone, A., 2015. Motility of a model bristle-bot: A theoretical analysis. *International Journal of Non-Linear Mechanics* 76, 233–239.
- [15] Copos, C., Mogilner, A., 2020. A hybrid stochastic–deterministic mechanochemical model of cell polarization. *Molecular biology of the cell* 31, 1637–1649.
- [16] DeSimone, A., Tatone, A., 2012. Crawling motility through the analysis of model locomotors: two case studies. *The European Physical Journal E* 35, 1–8.
- [17] Doedel, E.J., 1981. Auto: A program for the automatic bifurcation analysis of autonomous systems. *Congr. Numer* 30, 25–93.
- [18] Dolega, M., Zurlo, G., Le Goff, M., Greda, M., Verdier, C., Joanny, J.F., Cappello, G., Recho, P., 2021. Mechanical behavior of multi-cellular spheroids under osmotic compression. *Journal of the Mechanics and Physics of Solids* 147, 104205.
- [19] Doyle, A.D., Petrie, R.J., Kutys, M.L., Yamada, K.M., 2013. Dimensions in cell migration. *Current opinion in cell biology* 25, 642–649.
- [20] Doyle, A.D., Wang, F.W., Matsumoto, K., Yamada, K.M., 2009. One-dimensional topography underlies three-dimensional fibrillar cell migration. *The Journal of cell biology* 184, 481–490.
- [21] Drozdowski, O.M., Ziebert, F., Schwarz, U.S., 2021. Optogenetic control of intracellular flows and cell migration: A comprehensive mathematical analysis with a minimal active gel model. *Phys. Rev. E* 104. doi:10.1103/PhysRevE.104.024406.

- [22] DuChez, B.J., Doyle, A.D., Dimitriadis, E.K., Yamada, K.M., 2019. Durotaxis by human cancer cells. *Biophysical journal* 116, 670–683.
- [23] Estrada, R., Kanwal, R., 1989. Integral equations with logarithmic kernels. *IMA journal of applied mathematics* 43, 133–155.
- [24] Feng, J., Levine, H., Mao, X., Sander, L.M., 2019. Cell motility, contact guidance, and durotaxis. *Soft matter* 15, 4856–4864.
- [25] Gardel, M.L., Sabass, B., Ji, L., Danuser, G., Schwarz, U.S., Waterman, C.M., 2008. Traction stress in focal adhesions correlates biphasically with actin retrograde flow speed. *The Journal of cell biology* 183, 999–1005.
- [26] Giomi, L., DeSimone, A., 2014. Spontaneous division and motility in active nematic droplets. *Physical review letters* 112, 147802.
- [27] Hawkins, R.J., Piel, M., Faure-Andre, G., Lennon-Dumenil, A., Joanny, J., Prost, J., Voituriez, R., 2009. Pushing off the walls: a mechanism of cell motility in confinement. *Physical review letters* 102, 058103.
- [28] Hennig, K., Wang, I., Moreau, P., Valon, L., DeBeco, S., Coppey, M., Miroshnikova, Y., Albiges-Rizo, C., Favard, C., Voituriez, R., et al., 2020. Stick-slip dynamics of cell adhesion triggers spontaneous symmetry breaking and directional migration of mesenchymal cells on one-dimensional lines. *Science advances* 6, eaau5670.
- [29] Ippolito, A., Deshpande, V.S., 2021. Contact guidance via heterogeneity of substrate elasticity. *Acta Biomaterialia* .
- [30] Johnson, K.L., 1987. *Contact mechanics*. Cambridge university press.
- [31] Jülicher, F., Kruse, K., Prost, J., Joanny, J., 2007. Active behavior of the cytoskeleton. *Physics Reports* 449, 3–28. doi:10.1016/j.physrep.2007.02.018.
- [32] Karpenko, L., 1966. Approximate solution of a singular integral equation by means of jacobi polynomials. *Journal of Applied Mathematics and Mechanics* 30, 668–675. URL: <https://www.sciencedirect.com/science/article/pii/0021892867901037>, doi:[https://doi.org/10.1016/0021-8928\(67\)90103-7](https://doi.org/10.1016/0021-8928(67)90103-7).
- [33] Kruse, K., Joanny, J., Jülicher, F., Prost, J., 2006. Contractility and retrograde flow in lamellipodium motion. *Physical biology* 3, 130.
- [34] Kruse, K., Joanny, J.F., Jülicher, F., Prost, J., Sekimoto, K., 2005. Generic theory of active polar gels: a paradigm for cytoskeletal dynamics. *The European Physical Journal E* 16, 5–16.
- [35] Landau, L.D., Lifshitz, E., 1984. *Electrodynamics of Continuous Media*. volume 8 of *Course of Theoretical Physics*. Pergamon Press, Oxford. 2nd ed.
- [36] Larripa, K., Mogilner, A., 2006. Transport of a 1d viscoelastic actin–myosin strip of gel as a model of a crawling cell. *Physica A: Statistical Mechanics and its Applications* 372, 113–123.
- [37] Laurent, V.M., Kasas, S., Yersin, A., Schäffer, T.E., Catsicas, S., Dietler, G., Verkhovsky, A.B., Meister, J.J., 2005. Gradient of rigidity in the lamellipodia of migrating cells revealed by atomic force microscopy. *Biophysical journal* 89, 667–675.
- [38] Lavi, I., Meunier, N., Voituriez, R., Casademunt, J., 2020. Motility and morphodynamics of confined cells. *Physical Review E* 101, 022404.
- [39] Lelidis, I., Joanny, J.F., 2013. Interaction of focal adhesions mediated by the substrate elasticity. *Soft Matter* 9, 11120–11128.
- [40] Levental, K.R., Yu, H., Kass, L., Lakins, J.N., Egeblad, M., Erler, J.T., Fong, S.F., Csiszar, K., Giaccia, A., Weninger, W., et al., 2009. Matrix crosslinking forces tumor progression by enhancing integrin signaling. *Cell* 139, 891–906.

- [41] Lin, Y., 2010. A model of cell motility leading to biphasic dependence of transport speed on adhesive strength. *Journal of the Mechanics and Physics of Solids* 58, 502–514.
- [42] Lo, C.M., Wang, H.B., Dembo, M., Wang, Y.L., 2000. Cell movement is guided by the rigidity of the substrate. *Biophysical journal* 79, 144–152.
- [43] Löber, J., Ziebert, F., Aranson, I.S., 2014. Modeling crawling cell movement on soft engineered substrates. *Soft matter* 10, 1365–1373.
- [44] Maiuri, P., Terriac, E., Paul-Gilloteaux, P., Vignaud, T., McNally, K., Onuffer, J., Thorn, K., Nguyen, P.A., Georgoulia, N., Soong, D., et al., 2012. The first world cell race. *Current Biology* 22, R673–R675.
- [45] Mohammed, D., Charras, G., Vercruyssen, E., Versaevel, M., Lantoine, J., Alaimo, L., Bruyère, C., Luciano, M., Glinel, K., Delhaye, G., et al., 2019. Substrate area confinement is a key determinant of cell velocity in collective migration. *Nature Physics* 15, 858–866.
- [46] Mori, Y., Jilkine, A., Edelstein-Keshet, L., 2008. Wave-pinning and cell polarity from a bistable reaction-diffusion system. *Biophysical journal* 94, 3684–3697.
- [47] Oliveri, H., Franze, K., Goriely, A., 2021. Theory for durotactic axon guidance. *Physical Review Letters* 126, 118101.
- [48] Pasternak, P., 1954. On a new method of analysis of an elastic foundation by means of two foundation constants. *Gos. Izd. Lit. po Strait i Arkh* .
- [49] Peyton, S.R., Putnam, A.J., 2005. Extracellular matrix rigidity governs smooth muscle cell motility in a biphasic fashion. *Journal of cellular physiology* 204, 198–209.
- [50] Ponti, A., Machacek, M., Gupton, S.L., Waterman-Storer, C.M., Danuser, G., 2004. Two distinct actin networks drive the protrusion of migrating cells. *Science* 305, 1782–1786.
- [51] Protière, S., Boudaoud, A., Couder, Y., 2006. Particle–wave association on a fluid interface. *J. Fluid Mech.* 554, 85. doi:10.1017/S0022112006009190.
- [52] Putelat, T., Recho, P., Truskinovsky, L., 2018. Mechanical stress as a regulator of cell motility. *Physical Review E* 97, 012410.
- [53] Recho, P., Putelat, T., Truskinovsky, L., 2013. Contraction-driven cell motility. *Physical review letters* 111, 108102.
- [54] Recho, P., Truskinovsky, L., 2013. Asymmetry between pushing and pulling for crawling cells. *Physical Review E* 87, 022720.
- [55] Recho, P., Truskinovsky, L., 2016. Maximum velocity of self-propulsion for an active segment. *Math. Mech. Solids* 21, 263–278.
- [56] Ron, J.E., Monzo, P., Gauthier, N.C., Voituriez, R., Gov, N.S., 2020. One-dimensional cell motility patterns. *Phys. Rev. Research* 2, 2435. doi:10.1103/PhysRevResearch.2.033237.
- [57] Rubinstein, B., Fournier, M.F., Jacobson, K., Verkhovsky, A.B., Mogilner, A., 2009. Actin-myosin viscoelastic flow in the keratocyte lamellipod. *Biophysical journal* 97, 1853–1863.
- [58] Sabass, B., Schwarz, U.S., 2010. Modeling cytoskeletal flow over adhesion sites: competition between stochastic bond dynamics and intracellular relaxation. *Journal of Physics: Condensed Matter* 22, 194112.
- [59] Schreiber, C., Amiri, B., Heyn, J.C., Rädler, J.O., Faleke, M., 2021. On the adhesion–velocity relation and length adaptation of motile cells on stepped fibronectin lanes. *Proceedings of the National Academy of Sciences* 118, e2009959118.
- [60] Sens, P., 2013. Rigidity sensing by stochastic sliding friction. *EPL (Europhysics Letters)* 104, 38003.
- [61] Sens, P., 2020. Stick–slip model for actin-driven cell protrusions, cell polarization, and crawling. *Proc Natl Acad Sci USA* 117, 24670–24678. doi:10.1073/pnas.2011785117.

- [62] Shenoy, V.B., Wang, H., Wang, X., 2016. A chemo-mechanical free-energy-based approach to model durotaxis and extracellular stiffness-dependent contraction and polarization of cells. *Interface focus* 6, 20150067.
- [63] Tjhung, E., Marenduzzo, D., Cates, M.E., 2012. Spontaneous symmetry breaking in active droplets provides a generic route to motility. *Proceedings of the National Academy of Sciences* 109, 12381–12386.
- [64] Verkhovskiy, A.B., Svitkina, T.M., Borisy, G.G., 1999. Self-polarization and directional motility of cytoplasm. *Current Biology* 9, 11–S1.
- [65] Yam, P.T., Wilson, C.A., Ji, L., Hebert, B., Barnhart, E.L., Dye, N.A., Wiseman, P.W., Danuser, G., Theriot, J.A., 2007. Actin–myosin network reorganization breaks symmetry at the cell rear to spontaneously initiate polarized cell motility. *The Journal of cell biology* 178, 1207–1221.
- [66] Zhang, Z., Rosakis, P., Hou, T.Y., Ravichandran, G., 2020. A minimal mechanosensing model predicts keratocyte evolution on flexible substrates. *Journal of the Royal Society Interface* 17, 20200175.